

Wide Area X-ray Surveys for AGN and Starburst Galaxies

Andrew Ptak

Johns Hopkins University, Department of Physics and Astronomy

Abstract. While often the point sources in X-ray surveys are dominated by AGN, with the high sensitivity of modern X-ray telescopes such as Chandra and XMM-Newton normal/starburst galaxies are also being detected in large numbers. We have made use of Bayesian statistics for both the selection of galaxies from deep X-ray surveys and in the analysis of the luminosity functions for galaxies. These techniques can be used to similarly select galaxies from wide-area X-ray surveys and to analyze their luminosity function. The prospects for detecting galaxies and AGN from a proposed “wide-deep” XMM-Newton survey and from future wide-area X-ray survey missions (such as WFXT and eRosita) are also discussed.

Keywords: galaxies, active galactic nuclei, x-rays

PACS: 98.54.Ep, 98.62.Ve, 98.70.Qy

X-RAY SURVEYS

Extragalactic X-ray surveys are a powerful tool to study important source populations such as active galactic nuclei (AGN), clusters of galaxies, and, recently, normal galaxies [1]. In the bandpasses of Chandra and XMM-Newton, X-rays penetrate column densities up to $10^{23-24} \text{ cm}^{-2}$, and are therefore efficient at detecting moderately-obscured “Compton-thin” AGN. Compton-thick AGN (AGN with column densities of $> 10^{23-24} \text{ cm}^{-2}$) can also be detected in X-rays when prominent scattered emission is present (typically of order of $\sim 1\%$ of the intrinsic emission) [2] and can be detected in hard ($E > 10 \text{ keV}$) surveys [3]. Therefore X-ray surveys are essential for a complete census of AGN. Normal galaxies can now be detected in large numbers thanks to the high sensitivity of Chandra and XMM-Newton, however since they have low luminosities ($L_X < 10^{42} \text{ ergs s}^{-1}$), they are more difficult to detect than AGN.

X-rays from Normal/Starburst Galaxies

It has been known since the early 1980s that the X-ray emission of normal and starburst galaxies (galaxies with very high star-formation rates) are correlated with both the star-formation rate and stellar mass of the galaxies [4]. The physics behind this is that high-mass stars evolve rapidly (on time scales of 10^{6-8} years), and in turn explode as supernovae (SN). Occasionally these SN are detected in X-rays, however more often they heat the ISM to X-ray emitting temperatures (i.e., $T > 10^{6-7} \text{ K}$) and produce neutron stars and black holes in X-ray binaries. X-ray binaries where the companion is a high-mass star (high-mass X-ray binaries) also have short evolutionary time scales.

Therefore hot ISM and high-mass X-ray binaries track the current star-formation rate. Low-mass X-ray binaries have longer evolutionary time scales (on the order of Hubble times), and therefore track the integrated star-formation history of galaxies (i.e., the total stellar mass).

X-ray Galaxy Survey Strategies

There are several approaches to surveying specific sources types with low fluxes such as X-ray observations of galaxies. Deep, pencil-beam surveys of course probe to the faintest fluxes however due to the limited survey volume tend to result in low numbers of rare, high-luminosity objects. Wide area surveys (e.g., XMM-COSMOS) detect large numbers of AGN but are usually too shallow or survey too small of an area to detect significant numbers of galaxies. Another approach is to correlate large catalogs (e.g., the RC3 catalog or the SDSS) with archival data. For example, $\gtrsim 400$ galaxies have been detected in X-rays based on correlating the SDSS with the 2XMM catalog (see Parnau et al. these proceedings). We are pursuing this approach in the case of *Chandra* and *XMM-Newton* archival data by taking advantage of the XAssist pipeline processing of these data¹ and correlating the fields with the RC3 catalog. Note that by working with the original data rather than simply a source catalog we will be properly integrating the X-ray flux over the full RC3 ellipse for each galaxy, which is often larger than the telescope PSF, and also will be able to compute upper-limits for galaxies not detected in X-rays.

Finally we discuss the option of pursuing X-ray observations of statistically-complete samples that are not X-ray selected. We have been observing galaxies selected from the Nearby Field Galaxy Survey, which have very-well determined star formation rates [5]. We have received six XMM-Newton datasets and also included one serendipitous Chandra observation [6]. The X-ray/SFR correlation based on correlating the Chandra archive with the Kauffman SDSS galaxy catalog [7] is shown in Figure 1[8], with the X-ray NFGS data also plotted. The NFGS points are consistent with either the lower X-ray/SFR normalization implied by the X-ray detected SDSS galaxies, or a break in the X-ray/SFR correlation. Clearly a larger unbiased sample is needed.

BAYESIAN SELECTION AND ANALYSIS OF NORMAL GALAXIES IN DEEP X-RAY SURVEYS

In [9] and [10], normal/starburst galaxies were selected from the Chandra Deep Fields (CDF) using a Bayesian model selection methodology. Our motivation for employing this technique was to *directly take into account the X-ray measurement errors* which can be significant for X-ray sources at the flux limit of the survey.

¹ see <http://www.xassist.org>

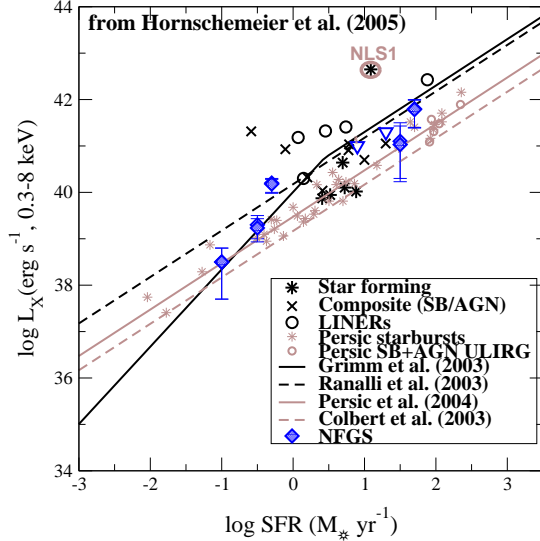


FIGURE 1. The X-ray/SFR correlation based on correlating SDSS galaxies and the Chandra archive [8], with data from XMM observations of the Nearby Field Galaxy Survey (NFGS) added.

Galaxy Selection

The most discriminating features for separating galaxies from AGN were found to be X-ray hardness ratio, $(H-S)/(H+S)$, where H and S are the numbers of photons above and below 2 keV, respectively, X-ray luminosity, and X-ray/optical flux ratio. In our analysis of GOODS data we also included the X-ray/near-IR flux ratio. We determined “parent” distributions for these parameters by selecting a sample of normal galaxies, type-1 AGN and type-2 AGN from the CDF South based on high quality optical spectroscopy, and then taking the mean and standard deviation (σ) for each parameter.

The posterior probability for observing the parameters θ , where here $\theta = \{HR, \log L_X, \log F_X/F_{\text{opt}}, \log F_X/F_{\text{NIR}}\}$ given the data D is given by Bayes’ theorem: $p_M(\theta|D) = p_M(\theta)p_M(D|\theta)/p_M(D)$. The M subscripts denote that this is assuming a given model M , here galaxies, type-1 AGN (AGN1) and type-2 AGN (AGN2). If multiple models are being considered, then the prior probability for each model must also be included. $p_M\theta$ are the “prior” distributions for the parameters for a given model M , for which we used the parent distributions discussed above. $p_M(D|\theta)$ is the likelihood function of observing the parameters θ given the data. Often $p_M(D)$ is considered to be a normalization constant since it does not depend on the model parameters θ , and is defined to be $p_M(D) = \int d\theta p_M(\theta|D)$. However $p_M(D)$ is also often (perhaps more precisely) considered to be the marginal likelihood or Bayesian evidence for the model M . The relative probability of two competing models given the data is then given by the

“Bayes Factor” or

$$\frac{p_{M_1}(D)}{p_{M_2}(D)} = \frac{\int d\theta p_{M_1}(\theta|D)}{\int d\theta p_{M_2}(\theta|D)} \quad (1)$$

Sources with $p_{\text{galaxy}}/p_{\text{AGN1}} > 1$ and $p_{\text{galaxy}}/p_{\text{AGN2}} > 1$ were selected as galaxies². Here we are assuming a flat prior on the numbers of sources for each model M , in other words we are assuming that the “true” number of normal/starburst galaxies, type-1 AGN and type-2 AGN are approximately equal.

Evolution

Evolution was observed qualitatively between the redshifts of 0.25 and 0.75 consistent with pure luminosity evolution, $L^*(z) = L^*(z=0)(1+z)^p$ with $p \sim 3$ by comparing the X-ray luminosity functions (XLFs) with the far-infrared luminosity functions [9]. Subsequently using GOODS data we fit the X-ray luminosity functions by using Markov-Chain Monte Carlo (MCMC) [10]. MCMC analysis results in a distribution of parameter values (the “chains”). This allows the direct visualization of posterior probabilities for important quantities, such as the change in L^* between the low and high redshift XLFs (Figure 2). Another key advantage of the Bayesian approach is that “derived” quantities such as luminosity density can be computed directly from the chain parameter values, allowing the posterior probabilities for these quantities to be visualized or summarized (i.e., with the mode as a “best-fit” value and the 68% confidence interval as the “error bar”) without questionable propagation of error [10, 11]. In future work we will be incorporating the additional 1 Ms of CDF-S data, as well as improving our MCMC analysis of the XLFs to also include VLA radio and Spitzer mid-IR data (both of which are star-formation rate indicators and will help discriminate galaxies from AGN).

WIDE-AREA X-RAY SURVEYS

XMM Wide-Area Surveys

While both XMM-Newton and Chandra are very sensitive X-ray telescopes, XMM-Newton has a larger field-of-view (FOV) than Chandra and is therefore more adept at wide-area surveys. While the total solid angle of 2XMM is large (hundreds of square degrees), its coverage is non-uniform and potentially biased since the field selection is not random. XMM-COSMOS is a wide-area survey covering 2 deg.² at an exposure of 40 ks per field, or a limiting point-source sensitivity of $\sim 5 - 10 \times 10^{-16}$ ergs s⁻¹ cm⁻² [12]. Here we briefly discuss a proposal to extend XMM-COSMOS out to 10 deg.² at a similar mean exposure per field³. This level of sensitivity would be sufficient to detect the (scattered) X-ray flux from Compton-thick AGN with a spectral energy distribution sim-

² In [10], a more conservative sample was selected with Bayes factors > 3 .

³ Submitted in the XMM AO-8 proposal round, PI David Alexander

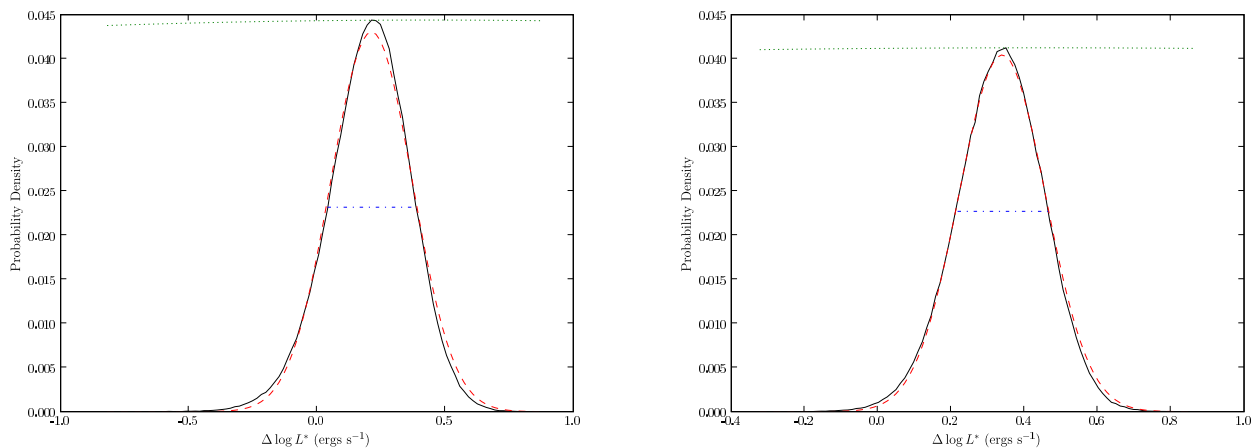


FIGURE 2. Posterior probability for the change in $\log L^*$ between the $z \sim 0.25$ and $z \sim 0.75$ for early-type (left) and late-type (right) galaxies. The solid (black) lines show the posterior probabilities, while the dashed (red) lines show Gaussian distributions with the same mean and standard deviation as the posteriors, and the dotted (green) lines show the prior distributions (\sim flat in these cases)

ilar to NGC 6240 at $z \sim 0.5 - 2.0$ (see Figure 3). This survey should result in 6000-8000 AGN being detected, ~ 1000 with at least 100 photons (sufficient for crude X-ray color analysis) and ~ 400 with at least 300 counts (sufficient for spectral analysis, including the detection of Fe-K lines). This survey would also detect $\sim 150 - 200$ AGN at $z > 3$ ($\sim 15 - 20$ at $z > 4$). We expect up ~ 300 normal/starburst galaxies would be detected, based on the Ranalli et al. logN-logS[13]. The field selection is in the Spitzer-SWIRE area, and the proposed X-ray data along with large amount of ancillary data from other wavebands available in these fields will allow us to study the coeval evolution of AGN and star formation over a wide range of redshift, environment and luminosity.

Future Missions

There are several proposed future missions dedicated to X-ray surveys. eRosita (extended Roentgen Survey with an Imaging Telescope Array) is an approved mission expected to fly aboard the Spectrum X-Gamma Mission, although the launch date appears to be uncertain⁴. eRosita will perform several surveys, including a nearly all-sky shallow survey. The Wide Field X-ray Telescope (WFXT) is a proposed medium-class NASA mission to similarly perform several surveys. The limiting flux and survey solid angle for both the WFXT and eRosita surveys are plotted in Figure 4. The numbers of AGN and clusters expected to be detected by eRosita and WFXT are shown in Figure 5. We expect on the order of $\sim 10^4$ normal/starburst galaxies to be detected in the eRosita surveys while $\sim 10^5$ galaxies should be detected in the WFXT surveys. Clearly either mission

⁴ <http://www.mpe.mpg.de/projects.html#erosita>

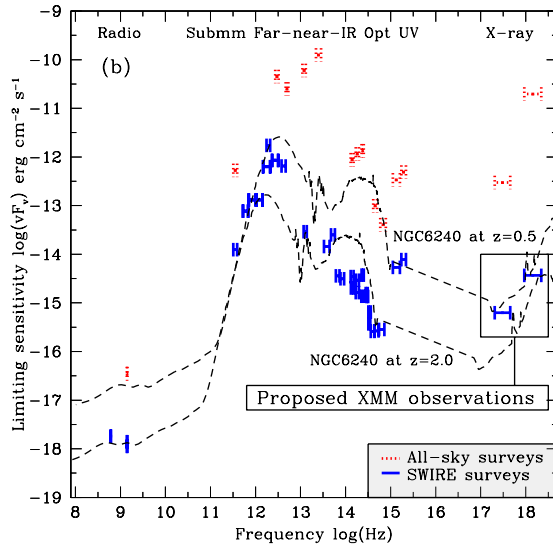


FIGURE 3. The SED of NGC 6240 (dashed curves, for redshifts of 0.5 and 2.0 and assuming a $L_X = 5 \times 10^{43}$ ergs s^{-1}) shown with the limiting fluxes of the SWIRE survey (blue), all-sky surveys (red) and the proposed XMM-Newton survey marked.

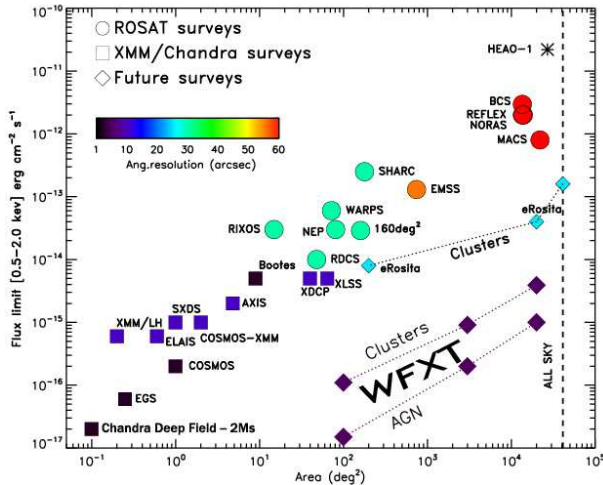


FIGURE 4. The limiting flux and solid angle of the surveys from the future missions WFXT and eRosita, where both the sensitivity to AGN (point sources) and clusters are shown, along with other X-ray surveys.

would drastically increase the numbers of X-ray detected sources and would be revolutionary. The high numbers of sources expected from WFXT is due to both a higher effective area and a smaller PSF (half-energy width of $\sim 7''$ for WFXT compared to the field-averaged PSF of $\sim 25 - 30''$ in the case of eRosita). WFXT also have the advantage of using a wide-field optical design [14], giving more uniform PSF and response across the 1 deg. FOV.

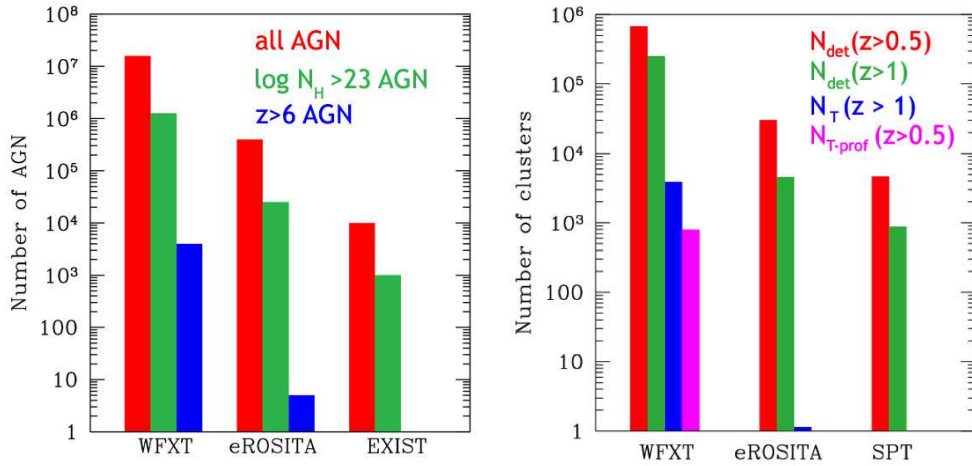


FIGURE 5. Expected numbers of AGN (left) and cluster of galaxies (right) to be detected by WFXT and eRosita. Also shown are the number of clusters of galaxies expected to be detected by the South Pole Telescope (SPT) via the Sunyaev-Zel’dovich effect.

ACKNOWLEDGMENTS

We acknowledge the support of NASA grants NNG04GE13G, NNG05GP14G, and NNG06GE59G.

REFERENCES

1. W. N. Brandt, and G. Hasinger, *Annual Reviews of Astronomy & Astrophysics* **43**, 827–859 (2005).
2. M. Cappi, and et al., *Astronomy & Astrophysics* **446** (2006).
3. L. Winter, R. Mushotzky, C. S. Reynolds, and J. Tueller, *Astrophysical Journal*, submitted (2008), astro-ph/0808.0461.
4. G. Fabbiano, *Annual Reviews of Astronomy & Astrophysics* **27**, 87–138 (1989).
5. L. J. Kewley, M. J. Geller, R. A. Jansen, and M. A. Dopita, *Astronomical Journal* **124**, 3135–3143 (2002).
6. A. Ptak, T. Heckman, C. Norman, A. Hornschemeier, L. Kewley, and A. Zezas, “The X-ray/SFR connection from X-ray observations of the nearby field galaxy sample,” in *ESAC faculty workshop on x-rays from nearby galaxies*, 2008, pp. 81–84.
7. G. Kauffmann, and et al., *Monthly Notices of the Royal Astronomical Society* **341**, 33–53 (2003).
8. A. E. Hornschemeier, T. M. Heckman, A. F. Ptak, C. A. Tremonti, and E. J. M. Colbert, *Astronomical Journal* **129**, 86–103 (2005).
9. C. Norman, and et al., *Astrophysical Journal* **607**, 721–738 (2004).
10. A. Ptak, B. Mobasher, A. Hornschemeier, F. Bauer, and C. Norman, *Astrophysical Journal* **667**, 826 (2007).
11. B. Kelly, X. Fan, and M. Vestergaard, *Astrophysical Journal* **682**, 874 (2008).
12. M. Salvato, and et al., *Astrophysical Journal in press* (2008), URL <http://arxiv.org/abs/0809.2098>, astro-ph/0809.2098, 0809.2098.
13. P. Ranalli, A. Comastri, and G. Setti, *Astronomy & Astrophysics* **440**, 23–37 (2005).
14. C. Burrows, R. Burg, and R. Giacconi, *Astrophysical Journal* **392**, 760 (1992).